24. Brunger, A. T. *et al.* Crystallography & NMR system: a new software suite for macromolecular structure determination. *Acta Crystallogr. D* **54,** 905–921 (1998).
25. Vagin, A. & Teplyakov, A. MOLREP: an automated program for molecular replacement. *J. Appl. Crystallogr.* **30,** 1022–1025 (1997).
26. Jones, T., Zou, J.-Y., Cowan, S. & Kjeldgaard, M. Improved methods for building protein models in electron density maps and the location of errors in these models. *Acta Crystallogr. A* **47,** 110–119 (1991).
27. Winn, M. D., Isupov, M. N. & Murshudov, G. N. Use of TLS parameters to model anisotropic displacements in macromolecular refinement. *Acta Crystallogr. D* **57,** 122–133 (2001).
28. Laskowski, R. A. *et al.* PROCHECK: a program to check the stereochemical quality of protein structures. *J. Appl. Crystallogr.* **26,** 283–291 (1993).
29. Carson, M. Ribbons. *Methods Enzymol.* **277,** 493–505 (1997).
30. Kraulis, P. J. A program to produce both detailed and schematic plots of protein structures. *J. Appl. Crystallogr.* **24,** 946–950 (1991).

Supplementary Information accompanies the paper on *Nature*'s website (**http://www.nature.com/nature**).

Acknowledgements We thank C. Ogata and M. Becker for assistance at beamlines X4A and X25, respectively, of NSLS at Brookhaven National Laboratory; A. Ullrich for supplying a human HER2 complementary DNA; P. Longo for technical assistance; T. Garrett, S. Yokoyama and colleagues for supplying preprints in advance of publication; S. Yokoyama for coordinates of the EGF–EGFR complex; M. Lemmon, K. Ferguson, M. Amzel, J. Berg, S. Bouyain and W. Yang for discussion and comments on the manuscript; A. Guarne for help with figures; and N. Davidson for assistance with Herceptin. This work was supported by the NIH and the HHMI.

Competing interests statement The authors declare that they have no competing financial interests.

Correspondence and requests for materials should be addressed to D.J.L. (e-mail: dleahy@jhmi.edu). Coordinates and structure factors are available from the Protein Data Bank under accession numbers 1N8Y (rat sHER2) and 1N8Z (human sHER2–Herceptin Fab complex).

Crystal structure of the specificity domain of ribonuclease P

Andrey S. Krasilnikov*, Xiaojing Yang*, Tao Pan† & Alfonso Mondragón*

* *Department of Biochemistry, Molecular Biology and Cell Biology, Northwestern University, Evanston, Illinois 60208, USA*
† *Department of Biochemistry and Molecular Biology, University of Chicago, 920 East 58th Street, Chicago, Illinois 60637, USA*

RNase P is the only endonuclease responsible for processing the 5′ end of transfer RNA by cleaving a precursor and leading to tRNA maturation[1,2]. It contains an RNA component and a protein component and has been identified in all organisms. It was one of the first catalytic RNAs identified[3] and the first that acts as a multiple-turnover enzyme *in vivo*. RNase P and the ribosome are so far the only two ribozymes known to be conserved in all kingdoms of life. The RNA component of bacterial RNase P can catalyse pre-tRNA cleavage in the absence of the RNase P protein *in vitro* and consists of two domains: a specificity domain and a catalytic domain[4,5]. Here we report a 3.15-Å resolution crystal structure of the 154-nucleotide specificity domain of *Bacillus subtilis* RNase P. The structure reveals the architecture of this domain, the interactions that maintain the overall fold of the molecule, a large non-helical but well-structured module that is conserved in all RNase P RNA, and the regions that are involved in interactions with the substrate.

Bacterial RNase P can be subdivided into two major types (A and B) on the basis of their sequence characteristics. The best-characterized RNase P molecules come from two bacteria, *Escherichia coli* and *B. subtilis*, which are paradigms for the A- and B-type molecules, respectively. The RNA component of bacterial RNase P (P RNA) consists of 350–450 nucleotides, whereas the protein component (P protein) is a small, basic protein of about 120 amino acids. In *B. subtilis* P RNA, the specificity domain (S domain) comprises nucleotides 86–239, and the catalytic domain (C domain) comprises the rest of the molecule (Fig. 1a). The S domain alone can bind pre-tRNA directly with micromolar affinity[6].

The overall structure of the specificity domain is shown in Fig. 1b together with a diagram illustrating the secondary structure of the molecule (Fig. 1c). The S domain consists of several distinct secondary structure modules, which were predicted from the P RNA sequence and by phylogenetic comparison[7,8]. Overall, the structure agrees very well with secondary structure predictions[8], cross-linking data[9] and Fe(II)-EDTA cleavage protection data[10] (see Supplementary Information). The most salient features of the structure are (1) a junction formed by the stacked P7, P10 and P11 and the stacked P8 and P9 helices; (2) the packing of the P10.1 and P12 helices through a GAAA tetraloop–tetraloop receptor interaction; and (3) an unusually folded module linking P11 and P12 (J11/12–J12/11) (orange in Fig. 1), which contains a large number of universally conserved nucleotides, and is stabilized without canonical Watson–Crick base pairing. Although the S domain forms a well-packed and compact structure, it is important to note that the P11 and P9 helices together with the J11/12–J12/11 module form a clamp-like opening that contains nucleotides involved in pre-tRNA binding and is large enough to accommodate the TψC stem-loop of a pre-tRNA molecule.

There are two molecules in the crystallographic asymmetric unit (1 and 2) related by a rotation of about 90°. It is unlikely that the crystallographic dimer observed is related to the dimer formed by the P RNA in the presence of the P protein in solution[11], as the intermolecular interactions observed in the crystal structure would lead to higher-order aggregates. The two molecules in the asymmetric unit are in slightly different conformations (see Supplementary Information). Molecule 1 has a disordered P12 helix and a partly disordered P10.1 helix (between bases A142 and G166). The tetraloop–tetraloop receptor interaction observed in molecule 2 is precluded in molecule 1 by crystal packing. Comparison of the two conformations suggests that the structure is built of relatively rigid structural elements and stabilized by a variety of interactions, such as stacking of helixes, stacking of bulged bases, and the tetraloop–tetraloop receptor interaction. The central element of the S domain is a rigid core (red in Fig. 1), which has a practically identical conformation in both molecules in the asymmetric unit (root-mean-square deviation (r.m.s.d.) = 0.63 Å). The core is formed by the continuous stacking of stems P10 and P11, together with the basal portion of the P10.1 stem. The base of the P10.1 stem includes a loop spanning U175 to A179 (see Fig. 2a). The phylogenetically conserved U175 and A179 form a reversed Watson–Crick base pair that stabilizes the loop and serves as the starting base pair for the P10.1 helix, helping to align the P10.1 stem with respect to the core. Two conserved adenosines in the loop, A177 and A178, enter the minor groove of the P7/P10 stack in a region including conserved base pairs G90–C235 and G132–C234. This type of interaction, between conserved adenosines in a loop and conserved G–C base pairs in a helix, has recently been termed an A-minor motif[12]. It includes contacts between the 2′-OH groups of the loop nucleotides with the 2′-OH groups of the helical residues similar to those in a ribose zipper[13]. The first four canonical Watson–Crick pairs in the P10.1 stem complete this portion of the rigid core. The second helix in the core is formed by the stacking of helices P10 and P11. This helix also stacks on stem P7 to form a large, continuous helix (Fig. 1). We do not include P7 in the rigid core because the P7/P10 stack is rather flexible (the angle between P7 and P10 differs by about 10° between molecules 1 and 2, as opposed to the P10/P11 stack in which the two molecules show identical conformations). The P11 stem includes bulged conserved adenosines A229 and A230 that do not form part of the helix.

The P7/P10/P11 helix is part of a large junction that also includes stacked helices P8 and P9. Figure 2b shows the topology of this complex junction. The general stacking of the helices is in agree-

ment with predictions based on modelling studies[8]. Non-Watson–Crick interactions in the region revealed by the crystal structure include the C134•(U181–A231) triplet, the stacking of bases A130 and A230 and the intercalation of A229 between G133 and C134. The last two interactions involve a sharp kink in the phosphate backbone to allow A229 to intercalate between G133 and C134. The backbone then folds back almost 180° so that A230 faces in the opposite direction to A229, and finally another kink resumes the regular helical structure (Fig. 2b, inset). Interestingly, bases involved in these interactions are conserved in bacterial P RNAs, underlining their importance in the correct folding and packing of the molecule as well as their involvement in substrate binding. The stacked bases A130 and A230 are especially interesting because they protrude from the body of the molecule and are protected from chemical modifications by the presence of substrate, both in *B. subtilis*[14] and in *E. coli*[15]. The stacked helix P8/P9 is capped on the P8 side by a large loop stabilized by a sheared base pair G97•A106, a reversed Hoogsteen base pair A98•U104 and a *trans* Sugar-edge/Watson–Crick base pair G100•A103.

Helix P11 is connected to a module formed by two large internal loops (J11/12–J12/11) consisting of A185–G196 and G217–C225 (orange in Fig. 1). These loops have a very similar structure in both molecules in the asymmetric unit (r.m.s.d. = 1.27 Å), although their relative position with respect to P11 is somewhat different, by about 10° (see Supplementary Information). The two chains in the module form a very closely packed structure (Fig. 3a) stabilized by an intricate network of interactions (major interactions are shown in Fig. 1c). There are no canonical Watson–Crick base pairs in this region, creating a large and stable structure without helical base pairing. The J12/11 strand (red in Fig. 3a) forms a loop that starts at the 3′ end of P12 and is stabilized by a reversed Hoogsteen pair, U218•A222. It then folds back to form a side-by-side base pair between adjacent nucleotides A222 and C223. The arrangement of these adjacent A and C nucleotides could be described as a dinucleotide platform, similar to an AA platform[16]. The J11/12 strand (blue in Fig. 3a) forms an S-shaped curve, stabilized by interactions between U189•G196 and A187•A191. Adjacent nucleotides A191 and C192 form another AC platform. In both cases, AC platforms are associated with a sharp, almost 180°, turn in the phosphate backbone.

The central part of P10.1, just above the central core region, contains four non-Watson–Crick base pairs with a bulged G168, as was predicted[8], and folds into a cross-strand A-stack joined to a bulged G motif[17] (Fig. 2c). The bulged G168 stacks on A194, which sticks out of the J11/12–J12/11 region. Stem P12 is a practically perfect eight-base-pair A-type helix, capped by a GAAA tetraloop. The tetraloop interacts with the tetraloop receptor in P10.1, as has been suggested previously[18]. The sequence of the tetraloop receptor,

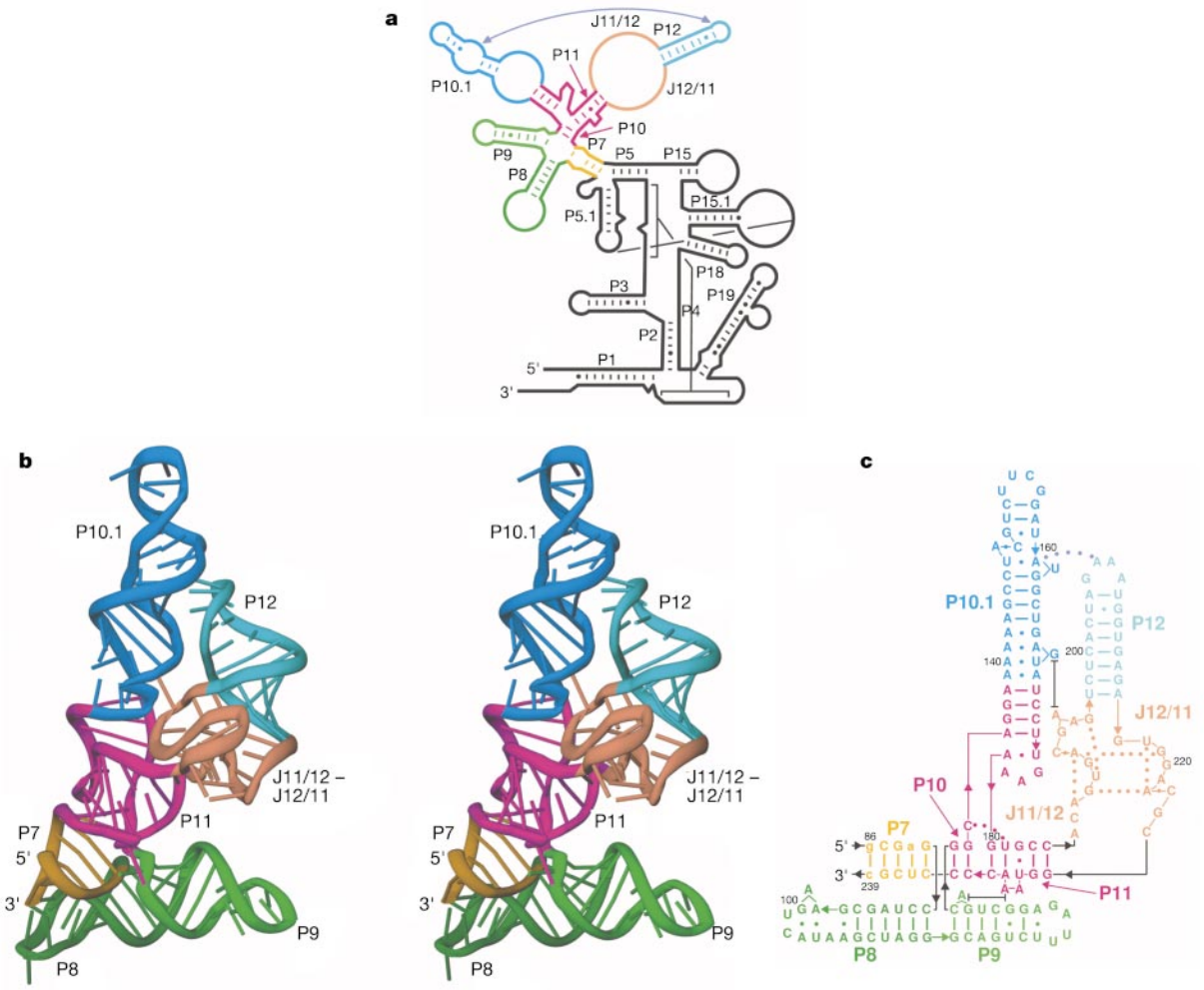

Figure 1 Structure of the S domain of *B. subtilis* RNase P RNA. **a**, Secondary structure of the entire P RNA. The P RNA consists of two well-defined domains, a specificity or S domain (shown in colours) and a catalytic or C domain (black). The diagram shows the secondary structure prediction and nomenclature according to ref. 30. Yellow, the P7 stem; green, the P8 and P9 stems; red, the central rigid core; blue, the distal part of P10.1; cyan, the P12 stem; orange, the J11/12–J12/11 module. **b**, Stereo ribbon diagram of the structure of the S domain. **c**, Sequence and secondary-structure diagram of the S domain. The nucleotides shown in lower-case letters correspond to mutations introduced in the crystallized fragment. Lines terminated by bars correspond to stacking interactions.

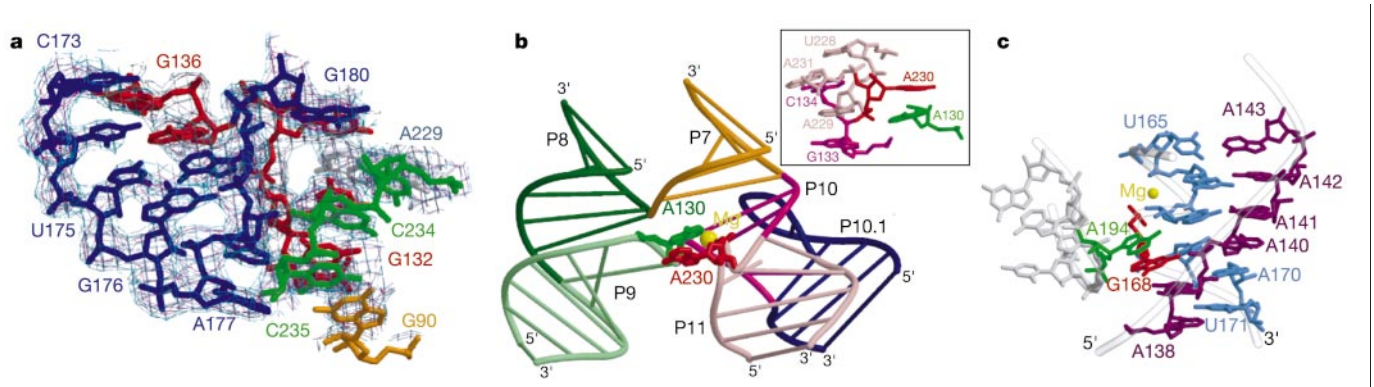

Figure 2 The central junction and the P10.1 helix. **a**, The loop at the basal part of the P10.1 stem interacts with the P7/P10 stack. Bases A177 and A178 in the loop interact with G–C base pairs at the junction of the P7 and P10 stems, forming an A-minor motif[12]. The solvent flattened experimental electron density map is shown at the 1.0σ and 1.5σ levels. **b**, The central part of the S-domain structure contains a junction bringing stems P7–P11 together. Two adenosines in the P11 stem bulge out; one of them, A230, stacks on A130 of the P9 stem. The other adenosine, A229, intercalates between G133 and C134 (inset). **c**, The central section of the P10.1 stem forms a cross-strand A-stack attached to a bulged G motif. Bulged G168 (red) stacks on A194 (green), which bulges out from J11/12 segment.

positioned in the upper part of P10.1, is the same as that found in group I introns[19], with one exception: the AA platform in the group I intron structure[13,16] is replaced with an AC platform in the *B. subtilis* S-domain tetraloop receptor, which is consistent with selection experiments *in vitro* indicating that AA and AC platforms in tetraloop receptors are interchangeable[20]. This replacement does not cause a substantial change in the geometry of the tetraloop–tetraloop receptor complex (r.m.s.d. = 0.91 Å).

The structure of the S domain of *B. subtilis* RNase P provides the basis for understanding the structure of other bacterial RNase P molecules, because sequence analysis suggests that the S domains of all bacterial P RNAs have a common core that comprises stems P7–P11 plus the J11/12–J12/11 module[21]. Alignment and comparison of 30 sequences of the S domain from B-type RNase P molecules[22], guided by the crystal structure of the *B. subtilis* S domain, clearly show that many of the conserved nucleotides are involved in interactions that are crucial for RNA folding (see Supplementary Information). The crystal structure of the S domain also allows important observations to be made for the S domains from A-type bacterial RNase P RNA, for which more than 300 sequences are known[22]. The major difference between the S domains of the A- and B-type bacterial RNase P molecules is the absence of the P10.1 stem and the addition of the P13 and P14 stems in the A-type RNase P molecules. It has been suggested previously[4] that the P13/P14 stems in A-type RNase P RNA, modelled as stacked helices[8], could have a similar role to the P10.1 stem in B-type RNase P RNA. Structure-based alignment of the A-type RNase P RNA sequences suggests that this could indeed be so. The position where the P13/P14 stems are inserted is located in the J12/11 strand. At this position in the S-domain structure the chain forms an exposed surface loop that faces the P10.1 helix. From this position in the J12/11 module, the P10.1 stem is only about 13 Å away. Therefore, P13/P14 could in principle form a long helix positioned in a similar orientation as the P10.1 stem. If the ends of the P13/P14 stems interact with the P12 and P8 stems, as suggested previously[7,8], the P13/P14 stem would indeed have an equivalent structural role to the P10.1 stem, giving the A- and B-type S domains very similar overall structures. The junction formed by stems P7–P11 is present in both bacterial types. In the B-type RNase P RNA, the P10.1 stem is inserted in the P10/P11 interface. Although A-type RNase P RNA does not have the P10.1 stem, there is a small bulged loop at the same position that might have an equivalent role in altering the P10/P11 interface. The J11/12–J12/11 module contains two of the five completely conserved regions in all RNase P molecules (Fig. 3b), and the structure of this module is expected to be very similar in all P RNAs from Bacteria, Archaea and Eukarya[21,23].

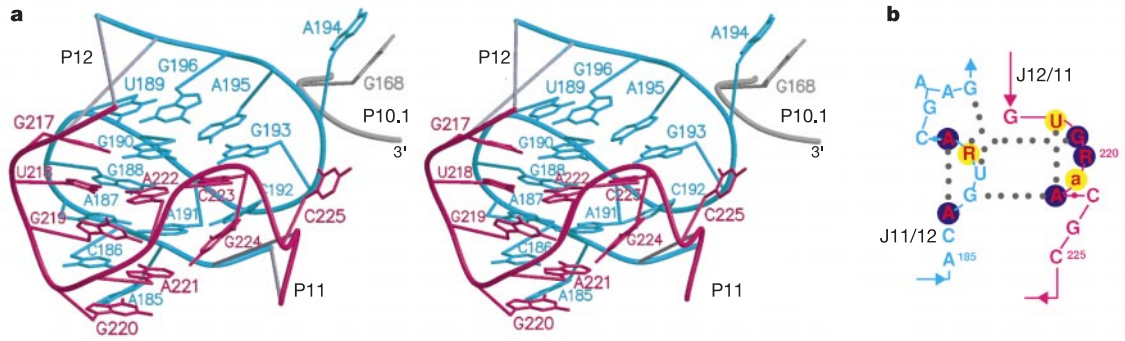

Figure 3 The J11/12–J12/11 module. **a**, The J12/11 segment (217–225) forms an internal loop (218–222) with G220 at its tip. The segment continues as the backbone makes a turn, forming an AC platform (A222–C223) and then joins the P11 stem. The J11/12 segment (185–196) is S-shaped and starts with a loop (nucleotides 187–191) which is structurally similar to the 218–222 loop (r.m.s.d. = 1.38 Å). Then the segment changes direction and forms an AC platform (A191–C192). The remaining part of the segment forms a smooth transition to the P12 stem. The A187–A191, U218–A222 and U175–A179 loops form a structural motif that is abundant in large RNA molecules (A.S.K. and A.M., unpublished observations). **b**, Conserved nucleotides in the J11/12–J12/11 module (circled). Sequence data[22] from Bacteria, Archaea and Eucarya were compared. Nucleotides in the yellow circle (lower-case letters), in the yellow circle (capitals) and circled in blue are at least 90%, 95% and 99% conserved, respectively.

One of the most remarkable interactions observed in the structure involves the stacking of bases that bulge out of the P9 and P11 stems. A pair of adenosines bulge out of the P11 helix, and one of them (A230 in *B. subtilis*) faces the P9 stem and stacks with an adenosine (A130) bulging out of the P9 stem (Fig. 2b). These nucleotides are involved in direct interactions with the pre-tRNA substrate[14,15]. The *B. subtilis* P RNA contacts at least three 2′-OH groups in the TψC stem and T-loop of pre-tRNA; for example, A230 directly interacts with the 2′-OH of nucleotide 62 in the TψC stem[24,25]. Consistent with this interaction is the observation that A230 in the structure of the S domain faces the solvent and the potential hydrogen acceptor, the N1 nitrogen of the base, is completely exposed. The bases of A130 and G220 are also exposed to the solvent and poised to interact with the substrate. Several of the contact sites in the pre-tRNA are in the same groove as the cleavage site but on the opposite face of the helix. Binding to one face of the TψC/acceptor stem by the S domain would therefore completely expose the cleavage site on the other side to be approached by the C domain.

The positions of the three nucleotides (A130, A230 and G220) directly involved in interactions with the pre-tRNA substrate are highlighted in Fig. 4. They belong to the region that has a clamp-like shape and forms a large opening that is more than 15 Å at its widest point. The bases of A230 and G220 are about 19 Å away, which is commensurate with the diameter of an RNA helix. The size of the aperture created by the S domain and the positions of the nucleotides involved in direct contacts make it tantalizing to suggest that the TψC stem and possibly the T-loop of pre-tRNA enter this region. Photoaffinity cross-linking experiments have shown that in *E. coli* RNase P, tRNA interacts with nucleotides in the P8–P9 stems[26], in agreement with the notion that the pre-tRNA is bound in this region. There is not enough experimental information to position the pre-tRNA in the S-domain structure unambiguously, but the size and shape of this region are ideal for interactions with the substrate. The high degree of sequence conservation in this region also suggests that all bacterial RNase P RNAs interact similarly with the substrate.

The regions protected from Fe(II)-EDTA cleavage in the presence of the P protein[5] and under conditions leading to holoenzyme dimerization *in vitro*[11] are also highlighted in Fig. 4. It is likely that only some of these regions are involved in binding to the P protein or in dimer contacts, and that the protection data also reflect changes in conformation due to the binding of P protein, contacts between P RNA and P RNA in the holoenzyme, or both. Nevertheless, it is striking that the P protein probably affects the structure in close proximity to the pre-tRNA-binding region, suggesting a direct coupling between pre-tRNA binding and P protein action.

The structure of the S domain of *B. subtilis* RNase P provides a molecular framework for studying the interactions that must occur between tRNA and the ribozyme during pre-tRNA processing. The structure is consistent with the available biochemical data for bacterial RNase P RNA and extends our understanding of RNase P structure across all taxonomic kingdoms. Furthermore, as an important addition to the still limited number of large RNAs of known structure, it advances our knowledge of the general principles of RNA structure and packing. □

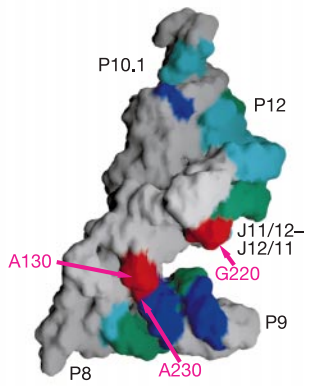

Figure 4 Surface representation of the S-domain structure. Three nucleotides (A130, A230 and G220) protected from chemical modifications by the substrate in *B. subtilis* RNase P[14] are shown in red. The position and distance between the nucleotides suggest that the clamp could serve to semi-enclose a large region of the substrate, for example the TψC stem. Regions protected from Fe(II)-EDTA cleavage owing to dimerization of the RNase P holoenzyme[11] (light blue), the presence of the protein[5] (dark blue) and the overlap of the two (green) are also shown. The protection experiments might not reflect the exact position of the protein or dimerization regions because conformational changes can affect the results, but the data serve to indicate that the dimerization and protein interaction regions are all located in the same face of the S domain and in proximity to the pre-tRNA-binding site.

Methods

The crystal structure of the S domain of *B. subtilis* RNase P was solved to 3.15 Å resolution from a two-wavelength multiwavelength anomalous diffraction experiment[27] with a Pb derivative. Refinement was done with Refmac5 (ref. 28) and CNS[29] without the use of non-crystallographic symmetry. The final R_{factor} and R_{free} values were 28% and 30.7%, respectively. The r.m.s.d. for bond lengths, angles and average *B* factor are 0.008 Å, 1.29° and 94.2 Å^2. The final model contains all RNA atoms except disordered bases 143–165 and 201–212 in molecule 1 and 121–124 in molecule 2. Only the phosphate backbone could be traced for bases 99 and 101 in both molecules. A combined model representing the entire S domain was built mostly from molecule 2, with bases 86–133 and 234–239 from molecule 1 and was used for all figures. Figures were prepared with Ribbons, Molscript, Bobscript and Grasp. For additional experimental details and references, see Supplementary Information.

Received 7 October; accepted 16 December 2002; doi:10.1038/nature01386.

1. Altman, S. & Kirsebom, L. A. in *The RNA World* (eds Gesteland, R. F., Cech, T. R. & Atkins, J. F.) 351–380 (Cold Spring Harbor Laboratory Press, Cold Spring Harbor, New York, 1999).
2. Frank, D. N. & Pace, N. R. Ribonuclease P: unity and diversity in a tRNA processing ribozyme. *Annu. Rev. Biochem.* **67,** 153–180 (1998).
3. Guerrier-Takada, C., Gardiner, K., Marsh, T., Pace, N. & Altman, S. The RNA moiety of ribonuclease P is the catalytic subunit of the enzyme. *Cell* **35,** 849–857 (1983).
4. Loria, A. & Pan, T. Domain structure of the ribozyme from eubacterial ribonuclease P. *RNA* **2,** 551–563 (1996).
5. Pan, T. Higher order folding and domain analysis of the ribozyme from *Bacillus subtilis* ribonuclease P. *Biochemistry* **34,** 902–909 (1995).
6. Qin, H., Sosnick, T. R. & Pan, T. Modular construction of a tertiary RNA structure: the specificity domain of the *Bacillus subtilis* RNase P RNA. *Biochemistry* **40,** 11202–11210 (2001).
7. Brown, J. W. *et al.* Comparative analysis of ribonuclease P RNA using gene sequences from natural microbial populations reveals tertiary structural elements. *Proc. Natl Acad. Sci. USA* **93,** 3001–3006 (1996).
8. Massire, C., Jaeger, L. & Westhof, E. Derivation of the three-dimensional architecture of bacterial ribonuclease P RNAs from comparative sequence analysis. *J. Mol. Biol.* **279,** 773–793 (1998).
9. Chen, J. L., Nolan, J. M., Harris, M. E. & Pace, N. R. Comparative photocross-linking analysis of the tertiary structures of *Escherichia coli* and *Bacillus subtilis* RNase P RNAs. *EMBO J.* **17,** 1515–1525 (1998).
10. Pan, T. Novel RNA substrates for the ribozyme from *Bacillus subtilis* ribonuclease P identified by *in vitro* selection. *Biochemistry* **34,** 8458–8464 (1995).
11. Barrera, A. *et al.* Dimeric and monomeric *Bacillus subtilis* RNase P holoenzyme in the absence and presence of pre-tRNA substrates. *Biochemistry* **41,** 12986–12994 (2002).
12. Nissen, P., Ippolito, J. A., Ban, N., Moore, P. B. & Steitz, T. A. RNA tertiary interactions in the large ribosomal subunit: the A-minor motif. *Proc. Natl Acad. Sci. USA* **98,** 4899–4903 (2001).
13. Cate, J. H. *et al.* Crystal structure of a group I ribozyme domain: principles of RNA packing. *Science* **273,** 1678–1685 (1996).
14. Odell, L., Huang, V., Jakacka, M. & Pan, T. Interaction of structural modules in substrate binding by the ribozyme from *Bacillus subtilis* RNase P. *Nucleic Acids Res.* **26,** 3717–3723 (1998).
15. LaGrandeur, T. E., Huttenhofer, A., Noller, H. F. & Pace, N. R. Phylogenetic comparative chemical footprint analysis of the interaction between ribonuclease P RNA and tRNA. *EMBO J.* **13,** 3945–3952 (1994).
16. Cate, J. H. *et al.* RNA tertiary structure mediation by adenosine platforms. *Science* **273,** 1696–1699 (1996).
17. Moore, P. B. Structural motifs in RNA. *Annu. Rev. Biochem.* **68,** 287–300 (1999).
18. Tanner, M. A. & Cech, T. R. An important RNA tertiary interaction of group I and group II introns is implicated in gram-positive RNase P RNAs. *RNA* **1,** 349–350 (1995).
19. Costa, M. & Michel, F. Frequent use of the same tertiary motif by self-folding RNAs. *EMBO J.* **14,** 1276–1285 (1995).
20. Costa, M. & Michel, F. Rules for RNA recognition of GNRA tetraloops deduced by *in vitro* selection: comparison with *in vivo* evolution. *EMBO J.* **16,** 3289–3302 (1997).
21. Chen, J.-L. & Pace, N. R. Identification of the universally conserved core of ribonuclease P RNA. *RNA* **3,** 557–560 (1997).
22. Brown, J. W. The Ribonuclease P Database. *Nucleic Acids Res.* **27,** 314 (1999).
23. Frank, D. N., Adamidi, C., Ehringer, M. A., Pitulle, C. & Pace, N. R. Phylogenetic-comparative analysis of the eukaryal ribonuclease P RNA. *RNA* **6,** 1895–1904 (2000).

24. Pan, T., Loria, A. & Zhong, K. Probing of tertiary interactions in RNA: 2′-hydroxyl-base contacts between the RNase P RNA and pre-tRNA. *Proc. Natl Acad. Sci. USA* **92,** 12510–12514 (1995).
25. Loria, A. & Pan, T. Recognition of the T stem-loop of a pre-tRNA substrate by the ribozyme from *Bacillus subtilis* ribonuclease P. *Biochemistry* **36,** 6317–6325 (1997).
26. Nolan, J. M., Burke, D. H. & Pace, N. R. Circularly permuted tRNAs as specific photoaffinity probes of ribonuclease P RNA structure. *Science* **261,** 762–765 (1993).
27. Hendrickson, W. A. Determination of macromolecular structures from anomalous diffraction of synchrotron radiation. *Science* **254,** 51–58 (1991).
28. Murshudov, G. N., Vagin, A. A. & Dodson, E. J. Refinement of macromolecular structures by the maximum-likelihood method. *Acta Crystallogr. D* **53,** 240–255 (1997).
29. Brunger, A. T. *et al.* Crystallography & NMR system: a new software suite for macromolecular structure determination. *Acta Crystallogr. D* **54,** 905–921 (1998).
30. Haas, E. S., Banta, A. B., Harris, J. K., Pace, N. R. & Brown, J. W. Structure and evolution of ribonuclease P RNA in Gram-positive bacteria. *Nucleic Acids Res.* **24,** 4775–4782 (1996).

Supplementary Information accompanies the paper on *Nature*'s website (http://www.nature.com/nature).

Acknowledgements We thank X. Liu and Y. Xiao for technical assistance, A. Changela, H. Feinberg, V. Grum and members of DND–CAT for help with data collection, and A. Changela, C. Correll, V. Grum, E. Sontheimer, B. Taneja and J. Wedekind for comments and suggestions. Research was supported by the NIH (to A.M.) and an NIH NRSA Fellowship to A.K. Support from the R.H. Lurie Cancer Center of Northwestern University to the Structural Biology Center is acknowledged. Portions of this work were performed at the DuPont–Northwestern–Dow Collaborative Access Team (DND–CAT) Synchrotron Research Center at the Advanced Photon Source (APS) and at the Stanford Synchrotron Radiation Laboratory (SSRL). DND–CAT is supported by DuPont, Dow and the NSF, and use of the APS is supported by the DOE. SSRL is operated by the DOE, Office of Basic Energy Sciences. The SSRL Biotechnology Program is supported by the NIH and the DOE.

Competing interests statement The authors declare that they have no competing financial interests.

Correspondence and requests for materials should be addressed to A.M. (e-mail: a-mondragon@northwestern.edu). Coordinates have been deposited in the Protein Data Bank under the accession code 1NBS.

retractions

A cytosolic catalase is needed to extend adult lifespan in *C. elegans daf-C* and *clk-1* mutants

J. Taub, J. F. Lau, C. Ma, J. H. Hahn, R. Hoque, J. Rothblatt & M. Chalfie

Nature **399**, 162–166 (1999).

We no longer have confidence in our observations associating a reduction in adult lifespan with a putative mutation in the *Caenorhabditis elegans* catalase gene *ctl-1* and therefore retract this paper. With the assistance of J. Liang and C. Keller, we have confirmed that *C. elegans* has multiple catalase genes (actually three in tandem) and that the original strain, TU1061, has decreased transcription of *ctl-1* messenger RNA. However, we have also found several errors, one identifying a single nucleotide deletion as the defect in the putative *ctl-1* mutation and others in the identification of strains carrying mutations in multiple genes. In particular, we have not seen the expected reduction in *ctl-1* mRNA in other strains tested. The longevity results obtained with these strains are therefore meaningless. We are grateful to our colleagues, particularly C. Kenyon and M. Crowder, for conveying to us their concerns about our results. □

Metal–insulator transition in chains with correlated disorder

Pedro Carpena, Pedro Bernaola-Galván, Plamen Ch. Ivanov & H. Eugene Stanley

Nature **418**, 955–959 (2002).

This Letter reported numerical simulations of one-dimensional disordered binary systems, and found a threshold value for the exponent characterizing the long-range power-law correlations of the system. Below this threshold, the system behaves as an insulator and above it, in the thermodynamic limit, the system behaves as a conductor. Unfortunately, we have now found that this observation was a consequence of the algorithm used to generate long-range correlations in binary chains, because above the threshold value of the exponent only a finite number of segments of atoms of the same type (A or B) exists, even in the thermodynamic limit of an infinitely large system. Thus, the system studied was not truly disordered. As a result, what we observed at the critical threshold value for the correlation exponent was not a transition from insulator to metal behaviour in a disordered system (as reported), but a transition from a disordered to an ordered system. For this reason, the authors retract the claim of a metal–insulator transition in the infinite binary chain with correlated disorder. The results are still valid that relate to the behaviour of a binary chain below the critical threshold value of the correlation exponent, and to large but finite system sizes (as found in the DNA example discussed in the Letter).

We thank L. Hufnagel and T. Geisel for drawing this to our attention. □

erratum

Wave-like properties of solar supergranulation

L. Gizon, T. L. Duvall Jr & J. Schou

Nature **421**, 43–44 (2003).

In Fig. 1, the units of frequency should be microhertz (μHz), not millihertz (mHz). In the US-printed issues, Fig. 3b appeared blurred. □

